MATERIALS CHEMISTRY
FRONTIERS

RESEARCH ARTICLE

View Article Online
View Journal | View Issue

Cite this: *Mater. Chem. Front.*, 2025, **9**, 838

On-surface gold-catalyzed hydroamination/cyclization reaction of alkynes†

Alejandro Jiménez-Martín, ‡[abc] Tatiana Munteanu,‡[d] Qifan Chen,‡[be] Simon Pascal,[df] Aura Tintaru,[d] Benjamin Mallada,[ab] Pingo Mutombo,[b] Olivier Siri,*[d] Pavel Jelínek*[ab] and Bruno de la Torre*[ag]

Received 2nd October 2024,
Accepted 16th January 2025

DOI: 10.1039/d4qm00866a

rsc.li/frontiers-materials

On-surface synthesis under ultra-high vacuum (UHV) conditions facilitates the fabrication of unique molecular compounds, replicating established in-solution protocols. However, the intramolecular hydroamination and cyclization (IHC) of alkynes on surfaces remain unexplored due to the challenges posed by the repulsion between the nitrogen lone pair and the alkyne π-system. Here we describe the first on-surface IHC of alkyne-functionalized molecular precursors in UHV environment on the Au(111) surface. Notably, the synthesis introduces two pyrrole groups into the quinoidal-based precursor, enabling the formation of two fused pyrrolo-benzoquinonediimine compounds not achievable in solution chemistry. To analyze the resulting reaction products, we utilized scanning tunneling microscopy and non-contact atomic force microscopy with single bond resolution, comparing these products to those obtained through traditional solution methods. In parallel to the experimental results, we provide a detailed computational description of the key role of single gold adatoms during the complete on-surface reaction.

Introduction

On-surface synthesis conducted under ultra-high vacuum (UHV) conditions is a relatively recent and highly active field of research that comes with a compelling approach for the atomically precise bottom-up fabrication of nanoarchitectures[1–3] mimicking known in-solution protocols.[4,5] This approach can be seen as an extension of heterogeneous catalysis, where the initial precursors, intermediate states, and reaction products all exist in an adsorbed state, typically under UHV conditions. Notably, its combination with surface science techniques, such as scanning probe microscopy, enables meticulous molecule-by-molecule characterization with single-bond precision[2,6] and isomer discrimination.[7] Recent advancements in on-surface synthesis have introduced innovative synthetic approaches that can rarely be achieved by conventional chemical means,[8,9] with numerous successful architectures being engineered, such as 1D covalent or organometallic oligomers and polymers,[10,11] 2D molecular networks,[12] non-covalently self-assembled structures,[13,14] nanoribbons[15,16] and even new carbon allotropes.[17,18]

One of the most appealing features of on-surface reactions is the access to remarkably original mechanisms and products, otherwise challenging to isolate under conventional chemical practices. Classic organic reactions have been adapted to the UHV conditions and interpreted within the newly established environment and conditions. Ullmann coupling, Bergman cyclization, Glaser coupling, Scholl reaction and ring-opening polymerization are just a few to mention.[1,2] Reactions based on engineering the properties of the alkyne triple bond are of particular interest because of its unique reactivity, which has enabled it to be used in various surface coupling reactions. Among these, the intriguing rearrangement of Bergman reaction[19] involving the intramolecular cyclization of an alkyne-containing precursor, remains one of the most extensively studied.[1,20,21] With their seminal work, de Oteyza *et al.* transferred the concept to metallic surfaces and have shown in

[a] *Regional Centre of Advanced Technologies and Materials, Czech Advanced Technology and Research Institute (CATRIN) Palacký University, Šlechtitelů 27, 78371 Olomouc, Czech Republic. E-mail: bruno.de@upol.cz*
[b] *Institute of Physics of the Czech Academy of Sciences, Cukrovanická 10, 16200 Prague, Czech Republic. E-mail: jelinekp@fzu.cz*
[c] *Faculty of Nuclear Sciences and Physical Engineering, Czech Technical University, Břehová 7, 11519 Prague, Czech Republic*
[d] *Aix Marseille Univ., CNRS UMR 7325 Centre Interdisciplinaire de Nanoscience de Marseille (CINaM), Campus de Luminy, 13288 Marseille cedex 09, France. E-mail: olivier.siri@univ-amu.fr*
[e] *Faculty of Mathematics and Physics, Charles University, V Holešovičkách 2/747, 18000 Prague, Czech Republic*
[f] *Nantes Université, CEISAM UMR 6230, CNRS, Nantes F-44000, France*
[g] *Nanomaterials and Nanotechnology Research Center (CINN) CSIC-UNIOVI-PA, 33940 El Entrego, Spain*

† Electronic supplementary information (ESI) available: Methods, synthesis of the materials, Fig. S1–S14, X-ray structure, NMR spectra, HRMS spectra, references. CCDC 2314122. For ESI and crystallographic data in CIF or other electronic format see DOI: **https://doi.org/10.1039/d4qm00866a**

‡ These authors contributed equally to this work.

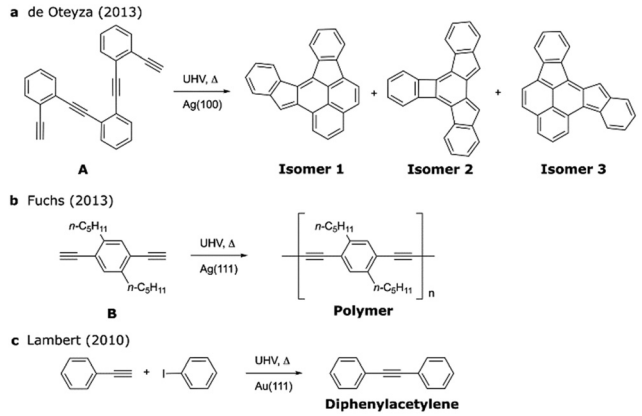

Scheme 1 Examples of on-surface reactions of alkyne-substituted precursors.

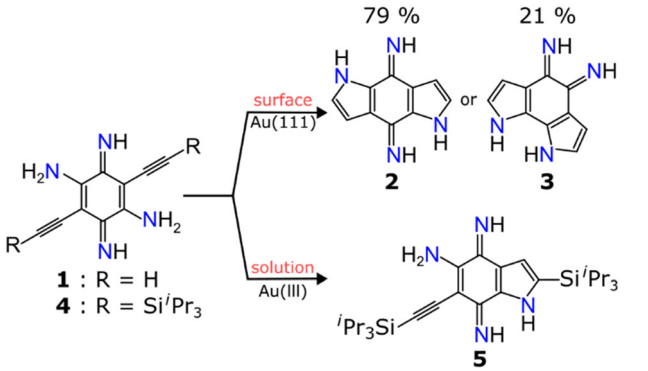

Scheme 2 Synthesis of fused N-heterocyclic derivatives. Representative scheme of the Au(0) on-surface synthesis reaction from molecular precursor **1** to the formation of final compounds **2** and **3** (top) and Au(III) solution-phase hydroamination/cyclization reaction from molecular precursor **4** to final product **5** (bottom).

a very elegant manner that the thermal activation of the ethynyl-bearing phenyl **A** on Ag(100) surface triggered an intramolecular Bergman cyclization, with the formation of three isomeric products[6] resulting from multiple reactions (Scheme 1).

Another alkyne-based reaction transferred from solution to surface chemistry is the Glaser coupling. This is a well-known and one of the oldest protocols employed in solution synthesis to obtain homocoupled diynes under copper catalysis.[19] The reaction was revitalized by the group of Ruben and Barth and by Fuchs and coworkers as a method for designing conjugated materials directly on surfaces.[22,23] Bisethynylarene monomers of type **B** (Scheme 1) upon annealing on Au(111), Ag(111) or Cu(111) surfaces were reported to undergo oligomerization, efficiently promoting the formation of linear polymeric chains with higher selectivity on Ag(111) substrate. The well-liked metal-catalyzed Sonogashira C–C coupling was also reported on Au(110) and Au(111) surfaces,[5,24,25] for instance generating diphenylacetylene as a cross-coupling product described by Lambert *et al.* from a reaction between phenylacetylene and iodobenzene (Scheme 1).

Despite the recent advancement in on-surface synthesis, examples of C–N bond formation through the intramolecular hydroamination/cyclization (IHC) reaction of alkynes are hitherto unknown probably because this reaction presents a considerable challenge due to the repulsion between a nitrogen lone pair and the alkyne π-system.[26] In solution, this reaction is a versatile and robust strategy for crafting multifunctional N-heterocycles[27,28] associated with substantial activation energy barriers that can be achieved through the use of expensive transition metal catalysts. Gold complexes, at different oxidation state, have thus emerged as highly effective catalysts for the electrophilic activation of alkynes, enabling nucleophilic additions to proceed under mild reaction conditions.[29] Notably, these gold catalysts selectively activate π-bonds of alkynes, facilitating the attack of various nucleophiles. Specifically, Au(I)-catalyzed hydroamination reactions have yielded notable success in formally adding N–H reagents onto triple bonds in both intermolecular[30,31] and intramolecular[32] contexts. Despite these advancements in solution, examples of on-surface IHC reactions are still missed.

In this study, we provide an innovative approach for the efficient synthesis of N-heterocyclic compounds *via* hydroamination and subsequent cyclization on Au(111) substrate and compare with that obtained by traditional methods in solution-phase chemistry. The precursor, 2,5-diamino-1,4-benzoquinonediimines (**1**, **4**), featuring a central quinoidal ring with two alkyne moieties and two amine functions, appears to be prime candidates for tandem hydroamination reactions of the alkynes, followed by cyclization under mild conditions (Scheme 2). On surface, the presence of single Au(0) adatoms nearby facilitates low-energy hydrogen migration from the amino group to the C≡C triple bond. This process evolves into fused N-heterocyclic compounds through an intramolecular cyclization reaction, leading to the high-yield production of compounds **2** and **3** (in a 4 : 1 ratio in favour of isomer **2**). Leveraging scanning tunneling microscopy (STM) and advanced bond-resolved non-contact atomic force microscopy (nc-AFM),[33] we effectively discerned the molecular configurations of reaction products formed on surfaces, unambiguously determining their structural changes. The reaction mechanism was further evaluated through density functional theory (DFT) calculations and quantum mechanics/molecular mechanics (QM/MM) calculations, rationalizing the occurrence of the final products. Interestingly, the same reaction was investigated in solution-phase chemistry with an Au(III) catalyst, showing the formation of the monocyclized compound **5** as model product of the unprecedented formation of pyrrolo fused benzoquinonediimine derivatives.

Results and discussion

Precursors **1** and **4** (Scheme 2) belong to a distinctive class of compounds characterized by a unique distribution of their π-electrons. Their molecular structure contains 12 π-electrons, but the molecule is best described as constituted of two independent π-subsystems containing 6 conjugated π-electrons (the

nitrogen lone pair is conjugated with the two double bonds), chemically linked *via* two C–C σ-bonds, but electronically not conjugated.[34,35] As a result, a peculiar reactivity can be expected through intramolecular hydroamination cyclization. In this work, both precursors were used to compare the hydroamination activation on the surface and using wet chemistry methods.

Reaction on surface

First, we introduce the on-surface IHC reaction. In a first attempt, we deposited intact molecules on Ag(111) substrate held at RT. The deposition is followed by the formation of a metalorganic pattern due to the C–H activation of both terminal alkynes and their subsequent coordination with silver surface adatoms (non-shown), thus indicating the need to use a less reactive substrate, like Au. As depicted in Fig. 1b, the deposition of precursor **1** (Fig. 1a) on Au(111) at room temperature results in the formation of spatially extended, close-packed islands, indicative of the high mobility of the species. The high-resolution nc-AFM image in the right panel of Fig. 1b elucidates the molecular composition of the stable organization of precursor **1**. Individual molecules are resolved by a central hexagon flanked by two elongated lines, corresponding to the alkyne groups, in concordance with simulation results depicted in Fig. 1b. Interestingly, rounded bright features are observed between the molecules, presumably indicating the presence of Au adatoms in the molecular framework.[36] This observation is consistent with the well-documented role of surface adatoms in directing the organization of molecular assemblies on surfaces.[37,38]

Subsequent elevation of the temperature of the surface to approximately 370 K initiated a pivotal transformation of the precursor, leading to the emergence of distinctly different molecular products and its subsequent self-assembly, as captured in the topographic image provided in Fig. 1c. The STM images prominently display single structures of the resulting products, which distinctly form one-dimensional chains guided by the intricate herringbone reconstruction of the surface Au(111). These molecular chains consist of two distinct molecular products, designated as type A (yield: 79%) and type B (yield: 21%) (see methods for calculation of yield in the ESI†), easily identifiable by their characteristic elongated and boomerang-like topographic shapes, respectively. Nc-AFM imaging of type A and type B products (Fig. 1d) unequivocally mirrors their chemical architectures. Each manifests a central hexagonal arrangement flanked by two pentagonal moieties in antisymmetric and symmetric configurations, respectively. The intricate intramolecular rearrangement potentially generates diverse isomeric variants for both molecular species considering the distribution of H atoms within the molecular structure.

The exact atomic structure of both products can be elucidated by combining a set of experimental and simulated

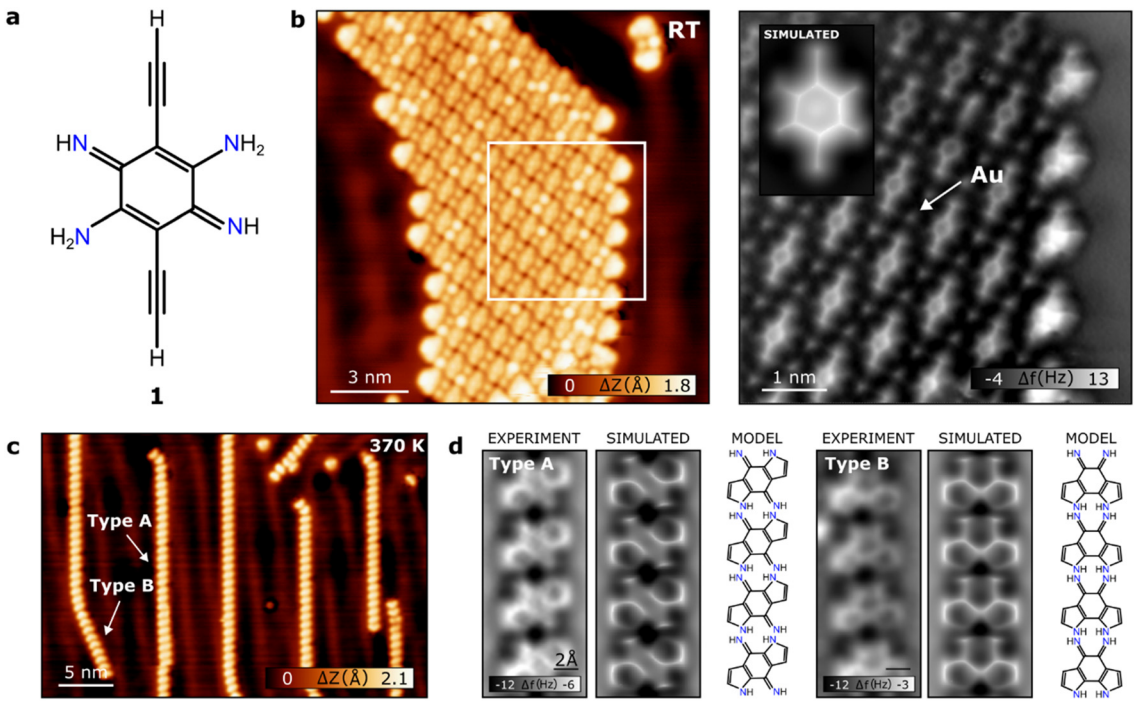

Fig. 1 On-surface characterization of N-heterocyclic compounds. (a) Chemical model of molecular precursor **1**. (b) STM topographic overview after deposition at RT of the molecular precursor **1** (left) (10 mV, 20 pA) and a close-up AFM image of the assembly surrounded by gold adatoms with a simulated AFM image of **1** (right). (c) STM topographic overview after annealing the sample at 370 K where two type A and B one-dimensional molecular structures are displayed. (0.1 V, 10 pA). (d) Experimental nc-AFM detailed image, simulated nc-AFM image and chemical model of final product **2** (type A) and **3** (type B).

nc-AFM images at different tip-sample distances. We conducted a series of nc-AFM simulations using fully optimized molecular structures obtained through total energy DFT calculations of potential isomeric variants of type A and B, considering the distribution of H atoms within the molecular structure. Fig. S1 (ESI†) presents the simulated nc-AFM images of the examined structures. Based on the agreement with experimental observations, we unambiguously identified the chemical structure of type A and type B molecules as products **2** and **3**, respectively (Fig. 1d). Moreover, we should note that this configuration of type A also has the lowest total energy between all considered structures, optimizing the strength of the dispersive and electrostatic intermolecular interactions (see Fig. S1 and S2, ESI†). In addition, the high-resolution nc-AFM images enable us to identify the supramolecular arrangement of both types of chains. While the type A chain formed by molecule **2** adopted a truncated configuration, molecule **3** organizes itself in a head-to-tail arrangement, culminating in chains characterized by specific intermolecular distances measuring 7.51 (±0.05) Å and 7.39 (±0.05) Å, respectively (see Fig. S3, ESI†). An in-depth analysis of consecutive sequences of products **2** and **3** revealed the presence of hydrogen bonds between the imine and amine units of adjacent molecules similarly to reported on quinoid molecule (2,5-diamino-1,4-benzoquinonediimine) deposited on Au(111).[13] The shape, whether linear or truncated, of the resulting chain was determined by the symmetric or antisymmetric configuration of the pyrrole moieties inherent in molecules **2** and **3**. Remarkably, we discovered that the molecular chains can be manipulated effortlessly by inducing lateral displacements with the STM tip (Fig. S4, ESI†). This investigation serves to probe the chemical stability of the hydrogen-bonded molecular chains. It was observed that segments could be easily displaced, with the molecules moving collectively while preserving their chain configuration. We observed that the precise positioning of pyrrole units significantly influences not only the molecular arrangement but also the electronic structure of the molecules. The calculated electronic gap for free-standing **2** and **3** shows a renormalization with the HOMO shifted closer to the Fermi level by ∼1 eV, reducing the molecular gap from 3.7 eV to ∼3 eV in good agreement with our experimental observations and calculations (see Fig. S5, ESI†).

Reaction pathway on surface

In order to gain a deeper understanding of the on-surface reaction mechanism, we carried out free-energy QM/MM simulations exploring different reaction pathways. Fig. 2 displays the optimal reaction pathways from precursor **1** towards products **2** and **3** according to our QM/MM simulations. These reaction schemes encompass hydrogen migration in tandem with the annulation or cyclization processes of both alkynes divided into two successive steps as discussed in the following.

Firstly, three distinct rotamers of the precursor, namely **IS1**, **IS2**, and **IS3**, were initially identified, with **IS2** being the most stable according to free-standing DFT calculations optimizing steric strain and electrostatic interaction between nitrogen lone pairs and hydrogen atoms (see Fig. S6, ESI†). However, the experimental situation provides a different scenario due to the presence of the gold surface. On the surface at moderated temperatures, there is an abundant amount of diffusing single gold atoms, so-called adatoms.[39] These gold adatoms have a neutral charge due to the presence of a gold surface underneath. Moreover, it has been recently demonstrated that these Au(0) adatoms may steer on-surface reactions.[40–42] The presence of the surface Au(0) adatoms on the Au(111) surface at RT, results in an average increase in the stability of **IS4** by about 0.35 eV (see Fig. S7, ESI†). In addition, the electrostatic potential map of **IS4** rotamer favours the presence of the single Au adatom nearby being electrostatically attracted by the nitrogen lone pair (Fig. S8, ESI†). Consequently, this rotamer becomes the most populated, assuming its dominant role in the reaction course.

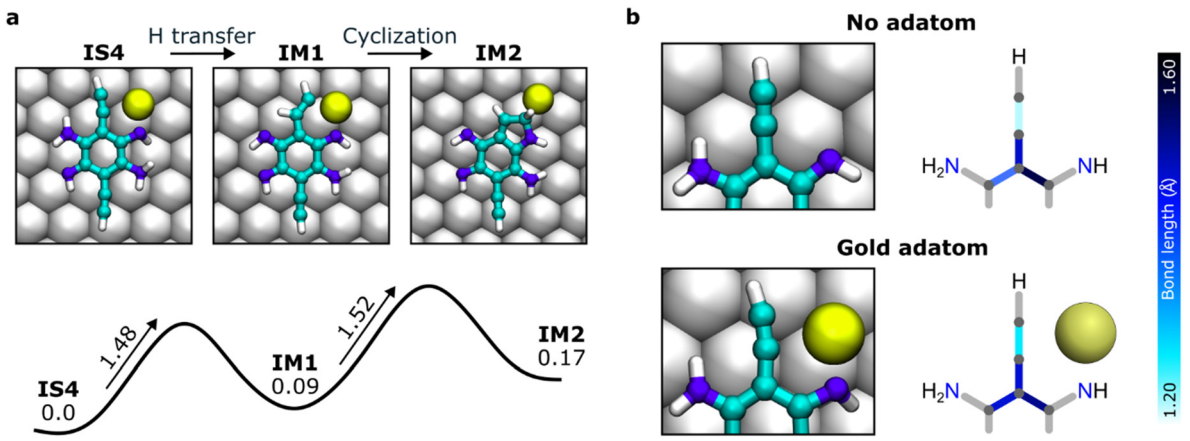

Fig. 2 Reaction pathway of the first hydroamination/cyclization. (a) Simulated snapshots and activation energies of the reaction steps from the initial state 1 (**IS4**), intermediate state 1 (**IM1**) and intermediate state 2 (**IM2**) of the ring closure. (b) Bond length analysis comparison for the effect of gold adatom in the hydrogen transfer step. The model shows an increment of the alkyne length with the presence of a gold adatom leading to a change in the character of the bond.

Thus, Fig. 2a shows the initial reaction step entails the migration of a single hydrogen atom from the amine moiety to the central carbon of the terminal alkyne leading to **IM1**. For this specific step, the presence of the single Au(0) adatom nearby plays a key role, reducing the energy barrier of the hydrogen transfer from 2.78 eV to 1.48 eV compared to the reaction without Au adatoms (as depicted in Fig. S9, ESI†). In contrast to our findings, dehydrogenation of the terminal alkyne typically results in the manifestation of Glaser-like coupling. This phenomenon has, indeed, been documented on Au(111)[22] under higher temperature conditions and on surfaces characterized by increased reactivity, such as Ag(111)[23,43] and Cu(111).[22]

We estimated reaction rates directly from the calculated barriers using the Arrhenius equation. For a barrier of 1.5 eV at 370 K, our calculations predict a reaction time of approximately 10 000 hours (not shown here) which is much longer than the experimental duration of 30 minutes. However, increasing the temperature to 400 K reduces the reaction time to around 20 minutes, aligning with experimental timescales. It is important to note that, in the experiment, the sample temperature was measured externally using a pyrometer, which introduces potential errors in the observed temperature (see methods in ESI†). These measurement uncertainties could result in a higher effective temperature than the reported 370 K, helping to reconcile the experimental timescales with our calculated barriers. Additionally, slight overestimations in the theoretical barriers, common in computational approaches, may also contribute to the apparent discrepancy.

Similarly, other competing dehydrogenation processes of the alkyne group, as well as hydrogen transfer within the alkyne group assisted by a single Au adatom, shown in Fig. S10 (ESI†), have a much larger activation barrier compared to the hydrogen transfer from the amine to central carbon atom of the alkyne segment. This modification renders the process more thermodynamically feasible at the experimentally relevant temperatures.

This primary step carries significant importance in unravelling the reaction mechanism. A detailed analysis of this reaction step reveals that the proximity of the Au adatom in **IS4** weakens the triple carbon bond on alkyne, as indicated by our DFT bond-length analysis (Fig. 2b and Fig. S11, ESI†). This prompts a redistribution of molecular charge, triggering the transfer of a hydrogen atom from the NH_2 to the central carbon in a sigmatropic reaction, culminating in forming a sp^3 central carbon (**IM1**). These findings strongly indicate a deviation from the conventional nucleophilic attack of the terminal alkyne,[44,45] providing an alternative mechanism on the surface. The efficacy of the metal catalysts in the hydroamination/cyclization in solution supports the involvement of a reaction pathway wherein the C≡C bond coordinates with the nucleophilic metal. Without this coordination, the amino group cannot effectively attack the alkyne carbon bonded to the phenyl group due to the molecular rigidity that inhibits bond bending.[46] Furthermore, the two-dimensional constraint imposed by the surface impacts the behaviour of individual gold adatoms and reactants, respectively, confining their movement and consequently limiting the effective coordination compared to that in solution chemistry. This first transformation serves as a pivotal precursor for understanding the subsequent steps of the reaction. It is succeeded by a cyclization process, resulting in the formation of the primary pyrrole moiety, leading to **IM2**, a common intermediate state for both **2** and **3** (see Fig. S12. ESI†).

The critical step determining the formation of either product **2** or **3** from **IM2** entails hydrogenation and cyclization processes of the second terminal alkyne, involving the amino group (refer to Fig. 3). At this bifurcation point, the positioning of the surrounding Au(0) adatom leads to different initial states (**IS′s**). Fig. S13 (ESI†) shows that **IS′1**, being 0.58 eV more favourable than the next one (**IS′3**), emerges as the leading state considered for further analysis. As shown in Fig. 3, the ground state **IS′1** undergoes a sigmatropic adatom-mediated hydrogen transfer from the NH_2 amino group to the central

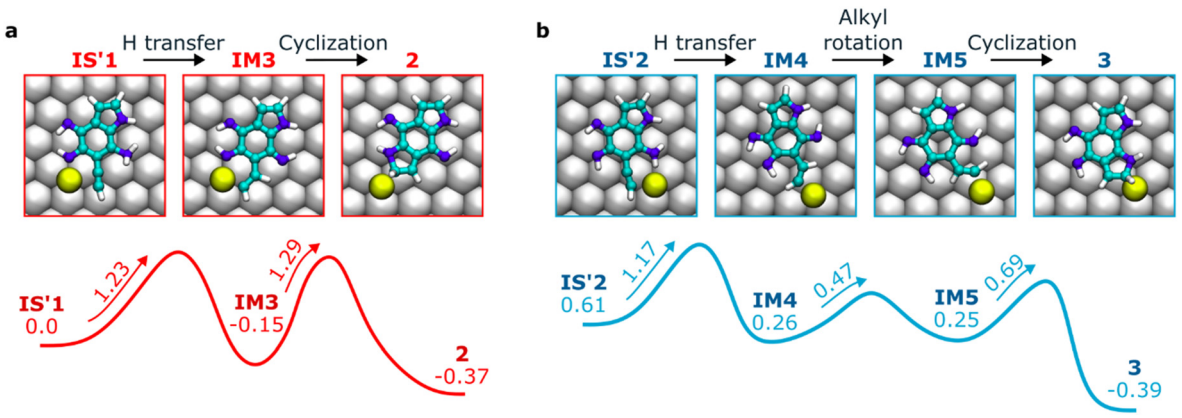

Fig. 3 Free-energy calculations of surface-catalysed reaction pathways of the second cyclization. (a) Top-view reaction snapshots and free energy profile (red) for the initial state (**IS′1**), intermediate state (**IM3**) and the final product (**2**) of the second ring cyclization for **2**. (b) Simulated images and energy reaction pathway (blue) for the initial state (**IS′2**), intermediate state 4 (**IM4**), intermediate state 5 (**IM5**) and the final product state (**3**) of the second ring closure for **3**.

carbon alkyne (**IM3**), induced by the proximity of a single Au(0) adatom, similar to the formation of the first pyrrole unit. A subsequent antisymmetric cyclization reaction leads to the formation of **2** with low energy barriers reachable with the mild conditions of the experiment, as depicted in Fig. 3a. On the other hand, the formation of **3** requires a unique starting point to enable the cyclization reaction (Fig. 3b).

Its notably lower yield compared to **2** implies a less likely reaction path for **3**. Hence, our focus shifts to **IS′s** states with elevated energy. Among **IS′2**, **IS′3** and **IS′4**, the former stands out, showing lower energy barriers, consistent with the experimental conditions. Proceeding from **IS′2**, the reaction closely mirrors **IS′1**, where Au(0) adatom mediates hydrogenation of the central alkyne, leading to the **IM4** state. This state marginally differs from **IM3** in the Au adatom's position and relative hydrogen conformations. At the subsequent stage, newly two channels appear, describing the pyrrole construction. The straightforward cyclization process yields again **2** with an energy barrier of 1.16 eV (see Fig. S12, ESI†). However, an alternate channel emerges with a lower energy barrier (0.47 eV) involving the alkyne's rotation guided by the gold adatom, leading to **IM5** and subsequent cycling toward the *ortho* position with a significantly lower energy barrier of 0.69 eV. Despite identifying other potential reaction pathways, this one is favored by approximately 0.24 eV (see Fig. S12, ESI†). The identified energy barrier giving rise to product **3** may provide a route for the selection of a pure (only **2**) or mixed (**2** and **3**) sample by fine-tuning the thermal energy reservoir in the experiment.

Reaction in solution

To provide a complete comparative of the on-surface hydroamination with traditional protocols, we investigated the reaction mechanism in solution from the closely related analogue **4**. We first synthesized **4** in 65% yield by using a protocol adapted from literature procedures[29,47,48] with a supplementary oxidation step before the final purification. Next, we envisaged from **4** the gold-catalyzed IHC by using $HAuCl_4{\cdot}3H_2O$ (0.3 equiv.). Interestingly, only one subunit of the molecule reacted, leading to the formation of **5** in 54% yield incorporating a single pyrrole unit (Fig. 4a). The ^{1}H NMR spectrum of **5** revealed an asymmetric molecule with a pyrrolic C–H proton at 6.63 ppm. ^{13}C NMR confirmed single cyclization, retaining the C≡C triple bond at 99 and 105 ppm and a correlation peak could be observed in ^{1}H–^{13}C HSQC spectrum corresponding to an olefinic CH (δ_C = 11.8 ppm; δ_H = 6.63 ppm). As expected for **5**, ^{1}H NOESY indicated spatial correlation between the indole ring's CH and Si^{i}Pr$_3$ protons (Fig. S19 and S20, ESI†). High-resolution mass spectrometry of **5** validated the monocyclization, showing a peak at m/z = 497.3490 Da corresponding to $C_{28}H_{49}N_4Si_2^+$ species (see more in the ESI†).

Finally, the structure of **5** was fully established by X-ray diffraction studies that clearly confirmed the formation of a fused pyrrolo-benzoquinonediimine derivative incorporating the C≡C triple bond (Fig. 4b and Fig. S14, ESI†). Further examination of the bond distances of **5** does not show the expected bond equalization for an aromatic pyrrole. This observation can be explained by the fused pyrrolo-benzoquinonediimine arrangement, in which the shared carbon–carbon bond functions as a C=C double bond, preserving the conjugation (rather than delocalization) of the π system within the benzoquinonediimine unit. These characteristics account for the absence of double cyclization in molecule **5** that can be rationalized by the nature of the catalyst.

In fact, $HAuCl_4$ is an anionic gold complex with an H^+ counterion, which might participate in an acid–base reaction

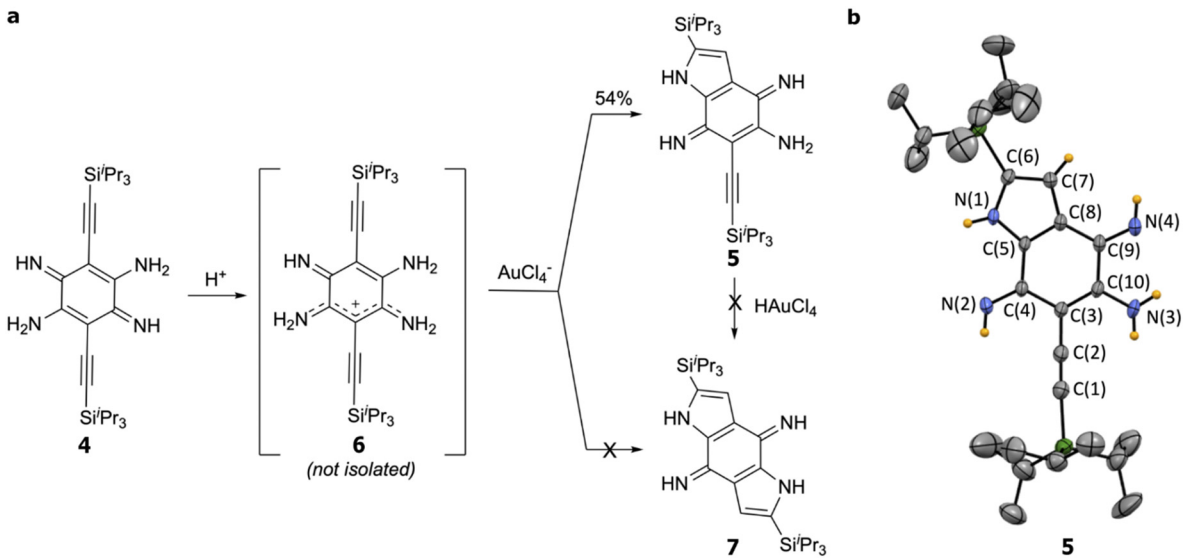

Fig. 4 In-solution synthesis of **5**. (a) Proposed formation of **5** *via* the protonation of **4** into intermediate **6**, followed by $AuCl_4$-catalyzed *N*-cyclization. The figure shows the non-formation of product **7** with $AuCl_4$- nor *via* second ring cyclization from **5** in the presence of $HAuCl_4^-$. (b) ORTEP view of **5**. Ellipsoid plots at 50% probability level. Bond lengths (Å): C(1)–C(2) = 1.185, C(2)–C(3) = 1.431, C(3)–C(4) = 1.466, C(4)–C(5) = 1.453, C(5)–N(1) = 1.356, N(1)–C(6) = 1.378, C(6)–C(7) = 1.394, C(7)–C(8) = 1.412, C(8)–C(9) = 1.445, C(9)–C(10) = 1.489, C(10)–C(3) = 1.378, C(5)–C(8) = 1.377, C(4)–N(2) = 1.287, C(9)–N(4) = 1.282, C(10)–N(3) = 1.346.

(protonation of an imine function in **4**) to generate the stabilized cationic species **6**, as depicted in Fig. 4a. This diminishes the nucleophilic character of the NH_2 function, thereby decreasing reactivity. To validate this, we sought to synthesize bicycled molecule **7** from monocyclized **4** under identical conditions (same catalyst), resulting in the complete recovery of the precursor. This underscores the influence of a ''parasitic'' acid–base reaction in our study.

Certainly, on-surface hydroamination reactions illustrate stark differences compared to the traditional synthesis in solution-phase. Specifically, the on-surface synthesis reveals a high yield with no evident side reactions compared to the moderate yield achieved in solution. Moreover, the on-surface reaction facilitates the complete cyclization of both alkynes, forming two pyrrole moieties per molecule, and conversely in solution, only one pyrrole unit was detected per molecule.

Conclusions

In summary, we have successfully demonstrated the unprecedented on-surface single-atom catalyzed hydroamination/cyclization reaction involving alkynes and amine groups for the fabrication of N-heterocyclic compounds **2** and **3**. The subsequent reaction, taking place on the surface, results in high-quality products through a cascade of hydrogen migration and hydroamination/cyclization processes, which were directly captured by nc-AFM. DFT and QM/MM calculations have verified the energetically favored *cis*-cyclization scenario, attributed to the influence of a single Au(0) adatom nearby, resulting in a highly efficient production. Direct comparison with traditional solution chemistry highlights striking differences with the on-surface hydroamination reaction since only the formation of the monocyclised species could be observed. Our results pave the way for further on-surface hydroamination reactions involving complex molecular structures, enhancing our understanding of single atoms in on-surface catalysis and aiming to fabricate functional N-heterocyclic compounds.

Author contributions

O. S., P. J. and B. T. conceived and designed the experiments. O. S., P. J. and B. T. supervised the project and led the collaboration efforts. A. J.-M., B. M. and B. T. carried out the SPM experiments, obtained the data and performed on-surface reactions. T. M, S. P. and O. S. synthesized the precursors and carried out the reactions in solution. A. T. performed all the NMR experiments in solution. The experimental data were analyzed by A. J.-M. and B.T.; and discussed by all the authors. Q. C., P. M. and P. J. performed the theoretical calculations. The manuscript was written by A. J.-M., O. S., P. J. and B. T. with contributions from all the authors.

Data availability

Data will be available on request. The crystallographic material for **5** can also be obtained from CCDC, the deposition number being CCDC 2314122.† More experimental details can be found in the ESI.†

Conflicts of interest

There are no conflicts to declare.

Acknowledgements

The work was supported by ERDF/ESF project TECHSCALE (No. CZ.02.01.01/00/22_008/0004587). We acknowledge the Research Infrastructure NanoEnviCz, supported by the Ministry of Education, Youth and Sports of the Czech Republic under Project No. LM2023066. B. T. acknowledges the financial support of Czech Science Foundation 23-06781M. P. J. and Q. Ch. acknowledge the financial support of Czech Science Foundation GACR 20-13692X and computational resources were provided by the e-INFRA CZ project (ID: 90254), supported by MEYS CR. O. S. thanks Spectropole (Aix-Marseille Univ.) for X-ray diffraction study and HRMS analyses. O. S. acknowledges the Ministère de la Recherche et de l'Enseignement supérieur, and the French research agency for the financial support of the project ANR-21-CE07-0058-01 CONDOR.

References

1 R. Lindner and A. Kühnle, On-Surface Reactions, *ChemPhysChem*, 2015, **16**, 1582–1592.
2 S. Clair and D. G. de Oteyza, Controlling a Chemical Coupling Reaction on a Surface: Tools and Strategies for On-Surface Synthesis, *Chem. Rev.*, 2019, **119**, 4717–4776.
3 A. Sweetman, N. R. Champness and A. Saywell, On-surface chemical reactions characterised by ultra-high resolution scanning probe microscopy, *Chem. Soc. Rev.*, 2020, **49**, 4189–4202.
4 P. A. Held, H.-Y. Gao, L. Liu, C. Mück-Lichtenfeld, A. Timmer, H. Mönig, D. Barton, J. Neugebauer, H. Fuchs and A. Studer, On-Surface Domino Reactions: Glaser Coupling and Dehydrogenative Coupling of a Biscarboxylic Acid To Form Polymeric Bisacylperoxides, *Angew. Chem., Int. Ed.*, 2016, **55**, 9777–9782.
5 V. K. Kanuru, G. Kyriakou, S. K. Beaumont, A. C. Papageorgiou, D. J. Watson and R. M. Lambert, Sonogashira Coupling on an Extended Gold Surface in Vacuo: Reaction of Phenylacetylene with Iodobenzene on Au(111), *J. Am. Chem. Soc.*, 2010, **132**, 8081–8086.
6 D. G. de Oteyza, P. Gorman, Y. C. Chen, S. Wickenburg, A. Riss, D. J. Mowbray, G. Etkin, Z. Pedramrazi, H.-Z. Tsai, A. Rubio, M. F. Crommie and F. R. Fischer, Direct Imaging of Covalent Bond Structure in Single-Molecule Chemical Reactions, *Science*, 2013, **340**, 1434–1437.

7 K. Morgenstern, Isomerization Reactions on Single Adsorbed Molecules, *Acc. Chem. Res.*, 2009, **42**, 213–223.
8 K. Kaiser, L. M. Scriven, F. Schulz, P. Gawel, L. Gross and H. L. Anderson, An sp-hybridized molecular carbon allotrope, cyclo[18]carbon, *Science*, 2019, **365**, 1299–1301.
9 B. Mallada, B. de la Torre, J. I. Mendieta-Moreno, D. Nachtigallová, A. Matěj, M. Matoušek, P. Mutombo, J. Brabec, L. Veis, T. Cadart, M. Kotora and P. Jelínek, On-Surface Strain-Driven Synthesis of Nonalternant Non-Benzenoid Aromatic Compounds Containing Four- to Eight-Membered Rings, *J. Am. Chem. Soc.*, 2021, **143**, 14694–14702.
10 V. M. Santhini, C. Wäckerlin, A. Cahlík, M. Ondráček, S. Pascal, A. Matěj, O. Stetsovych, P. Mutombo, P. Lazar, O. Siri and P. Jelínek, 1D Coordination π–d Conjugated Polymers with Distinct Structures Defined by the Choice of the Transition Metal: Towards a New Class of Antiaromatic Macrocycles, *Angew. Chem., Int. Ed.*, 2021, **60**, 439–445.
11 H. Denawi, M. Koudia, R. Hayn, O. Siri and M. Abel, On-surface synthesis of spin crossover polymeric chains, *J. Phys. Chem. C*, 2018, **122**, 15033–15040.
12 L. Lafferentz, V. Eberhardt, C. Dri, C. Africh, G. Comelli, F. Esch, S. Hecht and L. Grill, Controlling on-surface polymerization by hierarchical and substrate-directed growth, *Nat. Chem.*, 2012, **4**, 215–220.
13 A. Cahlík, J. Hellerstedt, J. I. Mendieta-Moreno, M. Švec, V. M. Santhini, S. Pascal, D. Soler-Polo, S. I. Erlingsson, K. Výbroný, P. Mutombo, O. Marsalek, O. Siri and P. Jelínek, Significance of nuclear quantum effects in hydrogen bonded molecular chains, *ACS Nano*, 2021, **15**, 10357–10365.
14 A. Jiménez-Martín, A. Gallardo and B. de la Torre, Coverage-modulated halogen bond geometry transformation in supramolecular assemblies, *Nanoscale*, 2023, **15**, 16354–16361.
15 Z. Chen, A. Narita and K. Müllen, Graphene nanoribbons: on-surface synthesis and integration into electronic devices, *Adv. Mater.*, 2020, **32**, 2001893.
16 P. Ruffieux, S. Wang, B. Yang, C. Sánchez-Sánchez, J. Liu, T. Dienel, L. Talirz, P. Shinde, C. A. Pignedoli, D. Passerone, T. Dumslaff, X. Feng, K. Müllen and R. Fasel, On-surface synthesis of graphene nanoribbons with zigzag edge topology, *Nature*, 2016, **531**, 489–492.
17 Q. Fan, L. Yan, M. W. Tripp, O. Krejčí, S. Dimosthenous., S. R. Kachel, M. Chen, A. S. Foster, U. Koert, P. Liljeroth and J. M. Gottfried, Biphenylene network: A nonbenzenoid carbon allotrope, *Science*, 2021, **372**, 852–856.
18 Y. Gao, F. Albrecht, I. Rončević, I. Ettedgui, P. Kumar, L. M. Scriven, K. E. Christesen, S. Mishra, L. Righetti, M. Rossmannek, I. Tavernelli, H. L. Anderson and L. Gross, On-surface synthesis of a doubly anti-aromatic carbon allotrope, *Nature*, 2023, **623**, 977–981.
19 C. Glaser, *Ber. Dtsch. Chem. Ges.*, 1869, **2**, 422–424.
20 B. Schuler, S. Fatayer, F. Mohn, N. Moll, N. Pavliček, G. Meyer, D. Peña and L. Gross, Reversible Bergman cyclization by atomic manipulation, *Nat. Chem.*, 2016, **8**, 220–224.
21 A. Riss, S. Wickenburg, P. Gorman, L. Z. Tan, H.-Z. Tsai, D. G. de Oteyza, Y.-C. Chen, A. J. Bradley, M. M. Ugeda, G. Etkin, S. G. Louie, F. R. Fischer and M. F. Crommie, Local electronic and chemical structure of oligo-acetylene derivatives formed through radical cyclizations at a surface, *Nano Lett.*, 2014, **14**, 2251–2255.
22 H.-Y. Gao, H. Wagner, D. Zhong, J.-H. Franke, A. Studer and H. Fuchs, Glaser coupling at metal surfaces, *Angew. Chem., Int. Ed.*, 2013, **52**, 4024–4028.
23 Y.-Q. Zhang, N. Kepčija, M. Kleinschrodt, K. Diller, S. Fischer, A. C. Papageorgiou, F. Allegretti, J. Björk, S. Klyatskaya, F. Klappenberger, M. Ruben and J. V. Barth, Homo-coupling of terminal alkynes on a noble metal surface, *Nat. Commun.*, 2012, **3**, 1286.
24 C. Sánchez-Sánchez, F. Yubero, A. R. González-Elipe, L. Feria, J. Fernández-Sanz and R. M. Lambert, The flexible surface revisited: adsorbate-induced reconstruction, homo-coupling, and Sonogashira cross-coupling on the Au (100) surface, *J. Am. Chem. C*, 2014, **118**, 11677–11684.
25 R. Chinchilla and C. Nájera, Recent advances in Sonogashira reactions, *Chem. Soc. Rev.*, 2011, **40**, 5084–5121.
26 B. Eftekhari-Sis, M. Zirak and A. Akbari, Arylglyoxals in synthesis of heterocyclic compounds, *Chem. Rev.*, 2013, **113**, 2958–3043.
27 M. Beller, J. Seayad, A. Tillack and H. Jiao, Catalytic Markovnikov and anti-Markovnikov functionalization of alkenes and alkynes: recent developments and trends, *Angew. Chem., Int. Ed.*, 2004, **43**, 3368–3398.
28 M. Patel, R. K. Saunthwal and A. K. Verma, Base-mediated hydroamination of alkynes, *Acc. Chem. Res.*, 2017, **50**, 240–254.
29 R. Dorel and A. M. Echavarren, Gold (I)-catalyzed activation of alkynes for the construction of molecular complexity, *Chem. Rev.*, 2015, **115**, 9028–9072.
30 K. Uchimoto, Y. Fukuda, K. Utimoto and H. Nozaki, Preparation of 2, 3, 4, 5-tetrahydropyridines from 5-alkynylamines under the catalytic action of Au (III), *Heterocycles*, 1987, **25**, 297.
31 E. Mizushima, T. Hayashi and M. Tanaka, Au (I)-catalyzed highly efficient intermolecular hydroamination of alkynes, *Org. Lett.*, 2003, **5**, 3349–3352.
32 M. Rudolph and A. S. K. Hashmi, Heterocycles from gold catalysis, *Chem. Commun.*, 2011, **47**, 6536–6544.
33 L. Gross, F. Mohn, N. Moll, P. Liljeroth and G. Meyer, The chemical structure of a molecule resolved by atomic force microscopy, *Science*, 2009, **325**, 1110–1114.
34 S. Pascal and O. Siri, Benzoquinonediimine ligands: Synthesis, coordination chemistry and properties, *Coord. Chem. Rev.*, 2017, **350**, 178–195.
35 O. Siri, P. Braunstein, M.-M. Rohmer, M. Bénard and R. Welter, Novel ''Potentially Antiaromatic'', Acidichromic Quinonediimines with Tunable Delocalization of Their 6π-Electron Subunits, *J. Am. Chem. Soc.*, 2003, **125**, 13793–13803.
36 M. N. Faraggi, N. Jiang, N. Gonzalez-Lakunza, A. Langner, S. Stepanow, K. Kern and A. Arnau, Bonding and charge

transfer in metal–organic coordination networks on Au (111) with strong acceptor molecules, *J. Phys. Chem. C*, 2012, **116**, 24558–24565.

37 J. V. Barth, G. Costantini and K. Kern, Engineering atomic and molecular nanostructures at surfaces, *Nature*, 2005, **437**, 671–679.

38 S. Stepanow, M. Lingenfelder, A. Dmitriev, H. Spillmann, E. Delvigne, N. Lin, X. Deng, C. Cai, J. V. Barth and K. Kern, Steering molecular organization and host–guest interactions using two-dimensional nanoporous coordination systems, *Nat. Mater.*, 2004, **3**, 229–233.

39 M. C. Tringides, *Surface Diffusion: Atomistic and Collective Processes*, Springer US, 1997, vol. 360.

40 J. I. Mendieta-Moreno, B. Mallada, B. de la Torre, T. Cadart, M. Kotora and P. Jelínek, Unusual Scaffold Rearrangement in Polyaromatic Hydrocarbons Driven by Concerted Action of Single Gold Atoms on a Gold Surface, *Angew. Chem., Int. Ed.*, 2022, **61**, e202208010.

41 J. Björk, C. Sánchez-Sánchez, Q. Chen, C. A. Pignedoli, J. Rosen, P. Ruffieux, X. Feng, A. Narita, K. Müllen and R. Fasel, The Role of Metal Adatoms in a Surface-Assisted Cyclodehydrogenation Reaction on a Gold Surface, *Angew. Chem., Int. Ed.*, 2022, **61**, e202212354.

42 A. Jiménez-Martín, F. Villalobos, B. Mallada, S. Edalatmanesh, A. Matěj, M. Cuerva, P. Jelínek, A. G. Campaña and B. de la Torre, On-surface synthesis of non-benzenoid conjugated polymers by selective atomic rearrangement of ethynylarenes, *Chem. Sci.*, 2023, **14**, 1403–1412.

43 A. Saywell, A. S. Browning, P. Rahe, H. L. Anderson and P. H. Beton, Organisation and ordering of 1D porphyrin polymers synthesised by on-surface Glaser coupling, *Chem. Commun.*, 2016, **52**, 10342–10345.

44 Y. Wang, Z. Wang, Y. Li, G. Wu, Z. Cao and L. Zhang, A general ligand design for gold catalysis allowing ligand-directed anti-nucleophilic attack of alkynes, *Nat. Commun.*, 2014, **5**, 3470.

45 S. M. A. Sohel and R.-S. Liu, Carbocyclisation of alkynes with external nucleophiles catalysed by gold, platinum and other electrophilic metals, *Chem. Soc. Rev.*, 2009, **38**, 2269–2281.

46 T. E. Müller, M. Grosche, E. Herdtweck, A.-K. Pleier, E. Walterm and Y.-K. Yan, Developing transition-metal catalysts for the intramolecular hydroamination of alkynes, *Organometallics*, 2000, **19**, 170–183.

47 D. Ye, J. Wang, X. Zhang, Y. Zhou, X. Ding, E. Feng, H. Sun, G. Liu, H. Jiang and H. Liu, Gold-catalyzed intramolecular hydroamination of terminal alkynes in aqueous media: efficient and regioselective synthesis of indole-1-carboxamides, *Green Chem.*, 2009, **11**, 1201–1208.

48 R. Heckershoff, S. Maier, T. Wurm, P. Biegger, K. Brödner, P. Krämer, M. T. Hoffmann, L. Eberle, J. Stein, F. Rominger, M. Rudolph, J. Freudenberg, A. Dreuw, A. S. K. Hashmi and U. H. F. Bunz, Cyclopentannulated Dihydrotetraazapentacenes, *Chem. – Eur. J.*, 2022, **28**, e202104203.

